Cation off-stoichiometry leads to high *p*-type conductivity and enhanced transparency in Co_2ZnO_4 and Co_2NiO_4 thin films

A. Zakutayev,* T. R. Paudel, P. F. Ndione, J. D. Perkins, S. Lany, A. Zunger,† and D. S. Ginley
National Renewable Energy Laboratory, Golden, Colorado 80401, USA

(Received 11 October 2011; revised manuscript received 27 December 2011; published 13 February 2012)

We explore the effects of cation off-stoichiometry on structural, electrical, optical, and electronic properties of Co_2ZnO_4 normal spinel and Co_2NiO_4 inverse spinel using theoretic and experimental (combinatorial and conventional) techniques, both at thermodynamic equilibrium and in the metastable regime. Theory predicts that nonequilibrium substitution of divalent Zn on nominally trivalent octahedral sites increases net hole density in Co_2ZnO_4. Experiment confirms high conductivity and high work function in Co_2NiO_4 and Zn-rich Co_2ZnO_4 thin films grown by nonequilibrium physical vapor deposition techniques. High *p*-type conductivities of Co_2ZnO_4 (up to 5 S/cm) and Co_2NiO_4 (up to 204 S/cm) are found over a broad compositional range, they are only weakly sensitive to oxygen partial pressure and quite tolerant to a wide range of processing temperatures. In addition, off-stoichiometry caused by nonequilibrium growth decreases the optical absorption of Co_2ZnO_4 and Co_2NiO_4 thin films, although the 500-nm thin films still have rather limited transparency. All these properties as well as high work functions make Co_2ZnO_4 and Co_2NiO_4 thin films attractive for technological applications, such as hole transport layers in organic photovoltaic devices or *p*-type buffer layers in inorganic solar cells.

DOI: 10.1103/PhysRevB.85.085204 PACS number(s): 73.61.Le, 71.55.Ht, 78.66.Li, 64.75.St

I. INTRODUCTION

A_2BO_4 compounds with spinel crystal structure[1] are a large and important group of ternary materials. Known applications of ternary spinels include water splitting, thermoelectricity, magnetism, transparent conductivity, and many others. In part, such a diversity of useful properties results from the existence of choices of cation coordination [both tetrahedral (Td) and octahedral (Oh)] and choices of cation valence (II, III, and IV) in spinel crystal structure, for example $[A_2{}^{+III}]_{Oh}[B^{+II}]_{Td}O_4{}^{-II}$ in the case of a perfect normal III/II spinel at 0 K.[2,3] Defects at finite temperatures may lead to deviation from the ideal 1:2:4 stoichiometry of spinels.[4] Surprisingly, dominant defects that may lead to off-stoichiometry in spinels are donor-like A^{+III}-on-Td antisite defects and acceptor-like B^{+II}-on-Oh antisite defects, in contrast to simple binary oxides known for vacancies or interstitials of metal and/or oxygen atoms.[5]

P-type doping of spinels, which is highly desirable for various applications, including optoelectronics, requires minimization of the electrical influence of donor-like A^{+III}-on-Td antisite defects and maximizing the electrical influence of acceptor-like B^{+II}-on-Oh antisite defects. Theoretically, two ways to minimize electrical influence of donor-like A^{+III}-on-Td antisite defects are (a) through minimizing its concentration (maximizing its formation enthalpy) or (b) through maximizing its ionization energy (lowering its transition level). For example, in the case of Co_2ZnO_4, in which donor-like Co-on-Td cation antisites are abundant but their Co^{+III}/Co^{+II} ionization energies are large,[5] high level of *p*-type conduction is achievable.[6] Similar effects occur in Rh_2ZnO_4 (Ref. 7) and Ir_2ZnO_4 (Ref. 8), all of which are spinels with d^6 electronic configuration.[9] Theoretically, two ways to maximize electrical influence of acceptor-like B^{+II}-on-Oh antisite defects are exactly opposite to those described above for donor-like A^{+III}-on-Td antisite defects, namely (a) through maximizing their concentration or (b) through minimizing their ionization energy. Experimentally, in order to achieve *p*-type dopability, concentration of B^{+II}-on-Oh can be maximized either by inducing B-rich off-stoichiometry using nonequilibrium growth or by choosing a B^{+II} element that naturally prefers Oh coordination. The ultimate endpoint of the second strategy is formation of the inverse spinel phase $[A^{+III}B^{+II}]_{Oh}[A^{+II}]_{Td}O_4{}^{-II}$, for example, Co_2NiO_4. If neither of these two strategies can be used to achieve high concentration of holes or if the B^{+II}-on-Oh transition level is too deep, extrinsic doping is required. More detailed discussion of these doping strategies was recently published in Ref. 10.

This paper discusses two strategies of *p*-type doping in spinels, namely inducing B-rich off-stoichiometry using nonequilibrium growth and choosing a B^{+II} element that naturally prefers Oh coordination. The first strategy is demonstrated in this paper on the example of Zn in Co_2ZnO_4 normal spinel[11] {i.e. $[Co^{+III}]_{Oh}[Zn^{+II}]_{Td}O_4{}^{-II}$}, and the second strategy is demonstrated on the example of Ni in Co_2NiO_4 inverse spinel[12] {i.e. $[Co^{+III}Ni^{+II}]_{Oh}[Co^{+II}]_{Td}O_4{}^{-II}$}. This paper provides (i) results and discussion of optical absorption and work function measurements of Co_2ZnO_4 (in addition to its conductivity), both of which are important properties of functional optoelectronic oxides, (ii) results and discussion not only for Co_2ZnO_4 but also for Co_2NiO_4, which is the promising material that was identified but not extensively studied in Ref. 10, and (iii) results and discussion of the influence of temperature (T) and oxygen partial pressure (pO_2) on properties of Co_2ZnO_4 and Co_2NiO_4.

Our experimental and theoretic results agree that (i) Zn-rich off-stoichiometry in Co_2ZnO_4 can be accommodated in excess of what equilibrium would mandate (Sec. III A), (ii) nonequilibrium high concentration of Zn can lead to significant enhancement of *p*-type conductivity (Sec. III B), (iii) replacing of Zn (prefers Td coordination) with Ni (prefers Oh coordination) and formation of Co_2NiO_4 inverse spinel leads to further increase in conductivity (Sec. III B). In addition, we experimentally show that optical absorption of both Co_2ZnO_4 and Co_2NiO_4 spinels decreases with increasing concentration of Zn and Ni, but their visible transparency remains rather limited (Sec. III B), and that both Co_2ZnO_4 and

Co_2NiO_4 thin films have quite high work functions and are promising for practical applications in various optoelectronic devices (Sec. III C). Theoretic and experimental details of methods used in this paper are described in Sec. II.

II. METHODS

A. Theory

We consider a phase pure A_2BO_4 in equilibrium with competing phases A_3O_4 and BO, such that:

$$\Delta H_{A_2BO_4} = 2\Delta\mu_A + \Delta\mu_B + 4\Delta\mu_O, \quad (1)$$

where $\Delta H_{A_2BO_4}$ is calculated formation energy of the A_2BO_4, and $\Delta\mu_O$, $\Delta\mu_A$, and $\Delta\mu_B$ are variable chemical potentials of atoms in the solid with respect to chemical potential of the standard state of elements. The ranges of variation of chemical potentials are defined from conditions of equilibrium with competing phases (i.e. O_2 gas, A_3O_4, and BO) as:

$$(3\Delta H_{A_2BO_4} - 2\Delta H_{A_3O_4} - 3\Delta H_{BO}) \leqslant \Delta\mu_O \leqslant 0, \quad (2)$$

$$(\Delta H_{A_2BO_4} - \Delta H_{BO} - 3\Delta\mu_O)/2 \leqslant \Delta\mu_A \leqslant (\Delta H_{A_3O_4} - 4\Delta\mu_O)/3, \quad (3)$$

$$(3\Delta H_{A_2BO_4} - 2\Delta H_{A_3O_4} - 4\Delta\mu_O)/3 \leqslant \Delta\mu_B \leqslant \Delta H_{BO} - \Delta\mu_O. \quad (4)$$

We determine (i) pO_2-vs-T thermodynamic stability region of Co_2ZnO_4 and Co_2NiO_4, (ii) T-vs-composition and pO_2-vs-composition thermodynamic stability regions of Co_2ZnO_4 and its net acceptor density as a function of pO_2, T and composition as described below:

(i) pO_2-vs-T thermodynamic stability regions of Co_2ZnO_4 and Co_2NiO_4, each of which is defined by two (oxidizing and reducing) boundaries, were calculated from maximal and minimal thermodynamically achievable chemical potentials of oxygen $\Delta\mu_O$ [Eq. (2)] using ideal gas law:

$$\Delta\mu_O(T, pO_2) = [H_O + C_P(T - T_O) - TS_O - Tc_P \ln(T/T_O) + K_BT \ln(pO_2/p_O)]/2, \quad (5)$$

where $c_p = 3.5k_B$, $k_B = 1.4 \times 10^{-23}$ J K^{-1}, and where tabulated values for oxygen at $T_0 = 298$ K and $p_0 = 1$ atm are $H_0 = 8700$ Jmol^{-1} and $S_0 = 205$ Jmol^{-1} K^{-1} (Ref. 13).

(ii) Composition, needed for the T-vs-composition and pO_2-vs-composition thermodynamic stability regions of Co_2ZnO_4 was determined using self-consistently calculated concentration of metal antisites (concentration of vacancies and interstitials was calculated to be negligible):

$$Zn/(Zn + Co) \approx \{[Zn_{Oh}] + [Zn_{Td}]\}/\{[Zn_{Oh}] + [Zn_{Td}] + [Co_{Oh}] + [Co_{Td}]\}, \quad (6)$$

where $[A_S]$ is the total concentrations of atom A on site S. Concentrations of $[Zn_{Oh}]$ and $[Co_{Td}]$ defects were calculated using Boltzman statistics:

$$[A_S]_q = D_q = N_S \times \exp(-\Delta H_{Dq}/k_BT), \quad (7)$$

where N_S is the concentration of available sites on the crystal lattice, and ΔH_{Dq} is the formation energy of a defect D in a charge state q. Formation energies of defects were calculated from first principles using:

$$\Delta H_{Dq} = (E_{Dq} - E_0) + \Sigma n_i(\Delta\mu_i + \mu_i^0) + q(E_{VBM} + E_f), \quad (8)$$

where n_i is the number of atoms i removed from the lattice to create a defect, E_{VBM} is energy of the valence band maximum, and E_f is Fermi energy with respect to E_{VBM}. Net acceptor density of Co_2ZnO_4 as a function of pO_2, T, and composition both in thermodynamic equilibrium [Eqs. (1)–(4)] and outside of it [$\Delta\mu_{Zn} > \Delta H_{ZnO} - \Delta\mu_O$ in Eq. (4)] were determined from concentrations [Eq. (7)] of all possible donors D and acceptors A as:

$$\delta N = \Sigma N_A - \Sigma N_D. \quad (9)$$

Since we are considering defect concentrations far beyond the dilute impurity limit, we take into account the appropriate normalization of the defect concentrations obtained by Eq. (7), as described in Ref. 14. For a given E_f, concentration of holes and electrons was calculated using the Fermi–Dirac statistics, and E_f was determined by numerical solution of the self-consistency problem defined by Eqs. (7) and (8) under the condition of overall charge neutrality of all positively and negatively charged defects and carriers. More details on the theoretical methods used to self-consistently calculate net acceptor density as a function of pO_2 and T (Ref. 13) and as a function of chemical composition,[15] both in thermodynamic equilibrium[16] and beyond solubility limits,[17] are published elsewhere.

Formation energies of Co_2ZnO_4, Co_2NiO_4, competing phases, and defects that are needed for the calculations described above were calculated from first principles within the density functional theory (DFT), employing the projector augmented-wave (PAW) method[18] as implemented in VASP code[19,20] and the Perdew–Burke–Ernzerhof (PBE) parameterization of the exchange correlation functional.[19] A soft pseudopotential for oxygen with the kinetic energy cutoff of 300 eV was chosen for ionic relaxation, whereas an energy cutoff up to 450 eV was used for the volume relaxation. Exchange and correlation effects beyond GGA were treated in rotationally invariant GGA + U formalism,[21] with U (3.0 and 2.9 eV for Co and Ni, respectively) determined in such a way that it correctly reproduces relative stability of competing binaries, such as Co_3O_4, CoO, NiO, and Ni_2O_3.[15] The defect calculations were performed in a 56-atom cubic cell with $2 \times 2 \times 2$ Monkhorst–Pack k points.[22] The energy of formation was corrected for the image charges, potential alignment, and band filling effects.[16] The band gap was corrected using *a posteriori* shift of the conduction band minimum. The dielectric constants necessary in the image charge correction were calculated using density functional perturbation approach[23] as implemented in VASP.

B. Experiments

Experiments on Zn-Co-O and Ni-Co-O (Co_2ZnO_4 and Co_2NiO_4 with varying Co content) described in this paper were performed using a combinatorial continuous-composition-spread cosputtering approach,[24] and the results for Ni-Co-O were verified using a conventional single-composition pulsed

laser deposition (PLD) approach. Zn-Co-O and Ni-Co-O continuous composition spread samples, aimed to study the effects of off-stoichiometry, were deposited using combinatorial radio-frequency (RF) cosputtering from 2-inch-diameter ZnO, NiO, and CoO targets located 20 cm (and at 45° angle) from the substrate. Powers applied to the targets were adjusted to create a chemical compositional spread across the combinatorial thin film samples in the chemical composition range of off-stoichiometry with respect to ideal A:B = 2:1 cation ratio in A_2BO_4 spinels. Stationary 51 × 51-mm fused silica substrates were heated to 250–650 °C, as verified by a thermocouple mounted on the surface of the sample. The depositions were performed in a vacuum chamber with the residual water base pressure of less than 10^{-9} atm, as verified by a residual gas analyzer. For the depositions, the chamber was filled with 2×10^{-5} atm of Ar/O_2 mixture with varying amount of O_2 in the range 10^{-6}–10^{-5} atm, in order to verify the dependence of physical properties of the samples on the pO_2 during the growth. After all the characterizations, the samples grown at 350 °C temperature in 10^{-5} atm oxygen partial pressure were sequentially annealed at 300–650 °C with 50 °C steps for 12 h per step in a box furnace filled with air ($pO_2 = 0.2$ atm), in order to verify the dependence of physical properties of the samples on annealing temperature and to check the trends observed for the depositions at different substrate temperatures. Single-composition Ni-Co-O samples with three different Ni:Co ratios were grown by pulsed laser deposition on 10 × 10-mm fused silica substrates heated to 300–500 °C placed 7 cm from the targets in a chamber with 10^{-10} atm base pressure filled with 2.6×10^{-6} atm of oxygen without addition of argon. Ni-Co-O targets with Ni/(Ni + Co) = 0.33, 0.38, and 0.43 were ablated using 248-nm excimer laser beam with 2.5 J/cm^2 energy density and 10 Hz repetition rate. In addition, samples grown at room substrate temperature at otherwise equal conditions were sequentially annealed at 300–500 °C in air with 100 °C steps for 1 h per step.

Each of the combinatorial samples was automatically mapped at 44 points (4 × 11 grid) to find the properties of the material as a function of off-stoichiometry. The samples were routinely measured using x-ray fluorescence (XRF), x-ray diffraction (XRD), optical spectroscopy, four-point probe sheet resistance mapping, and Kelvin-probe (KP) mapping. X-ray fluorescence spectra were collected using Roentgenanalytic maXXi 5/PIN instrument and analyzed using MTF-FP software to obtain both chemical composition and the thickness of the samples. The accuracy of the thickness measurement was verified by depositing an equivalent sample patterned with a shadow mask and by measuring the thickness of each of the individual 44 features using a profilometer. X-ray diffraction patterns of Cu Kα radiation were collected using a proportional 2D detector. The diffraction peaks were assigned based on the Co_2ZnO_4, Co_2NiO_4, Co_3O_4, ZnO, and NiO reference diffraction patterns obtained from the Inorganic Crystal Structure Database (ICSD). Optical spectra were mapped in the 300–2000-nm range using a fiber-optics-based spectrometer with normally incident angle of light generated by deuterium and tungsten/halogen light sources and collected using Si and InGaAs detector arrays. The measured transmittance (T) and reflectance (R) spectra were converted into the absorption coefficient α using the relationship $\alpha = -\ln[T/(1 - R)]/d$, where d is the film thickness.[25] Sheet resistance mapping was performed using a collinear head with 1-mm distance between four probes. P-type electrical conduction was confirmed by a measured positive sign of Seebeck coefficient.[26] Kelvin-probe mapping with 1-mm-diameter gold-coated probe was used to determine the work function of Zn-Co-O and Ni-Co-O combinatorial samples. The samples were placed in an ambient atmosphere and grounded during the work function measurement. The Kelvin-probe mapping system was calibrated both before and after every mapping run using Au and Al standards with reference 5.1 and 4.1 eV work function, respectively. Each of the single-composition Ni-Co-O samples was also characterized using aforementioned XRF, XRD, and four-point probe sheet resistance measurements.

III. RESULTS AND DISCUSSION

A. Cation off-stoichiometry

In thermodynamic equilibrium, Co_2ZnO_4 normal spinel has a wider pO_2-vs-T stability range than Co_2NiO_4 spinel. The results of the pO_2-vs-T stability range calculation [Eq. (5)] that assume thermodynamic equilibrium conditions [Eqs. (1)–(4)] are shown in Fig. 1. These theoretical results indicate that growth of Co_2ZnO_4 material should be possible both in high vacuum and at ambient atmospheric pressure, but growth of Co_2NiO_4 in these conditions should be difficult. For example, Co_2ZnO_4 is thermodynamically stable in a single spinel phase up to 1000 °C at $pO_2 = 0.2$ atm and up to 600 °C at $pO_2 = 10^{-5}$ atm [Fig. 1(a)], but Co_2NiO_4 pO_2-vs-T stability range is limited to about room temperature even

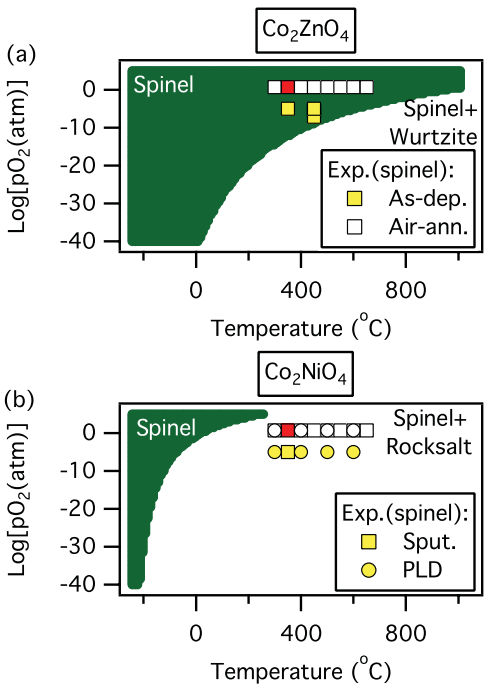

FIG. 1. (Color online) Theoretic thermodynamic equilibrium pO_2-vs-T stability range (marked in green/gray) for (a) Co_2ZnO_4 and (b) Co_2NiO_4. Experimental growth conditions are marked by symbols. Red/dark gray symbols indicate samples shown in Fig. 2. The legend in (a) applies to both (a) and (b).

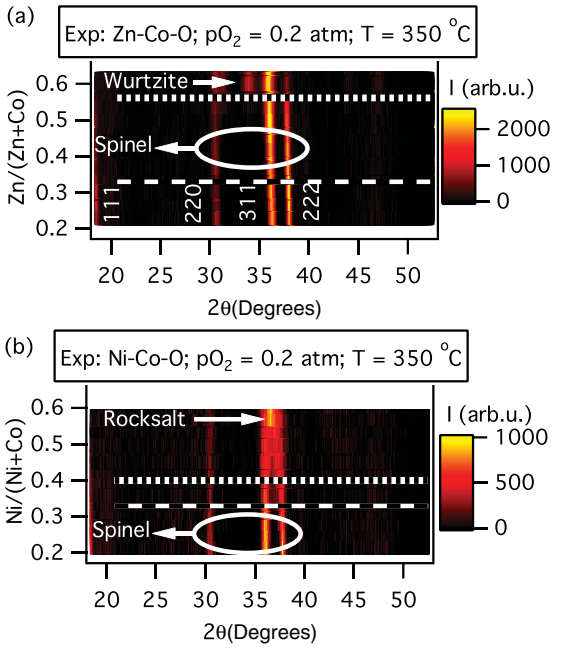

FIG. 2. (Color online) Experimental x-ray diffraction maps for (a) Zn-Co-O and (b) Ni-Co-O annealed at 350 °C in air (red/dark gray symbols in Fig. 1). The dashed line indicates a nominal 2:1 spinel cation ratio. The dotted line indicates an onset of phase separation. Vertical labels indicate XRD peak assignments.

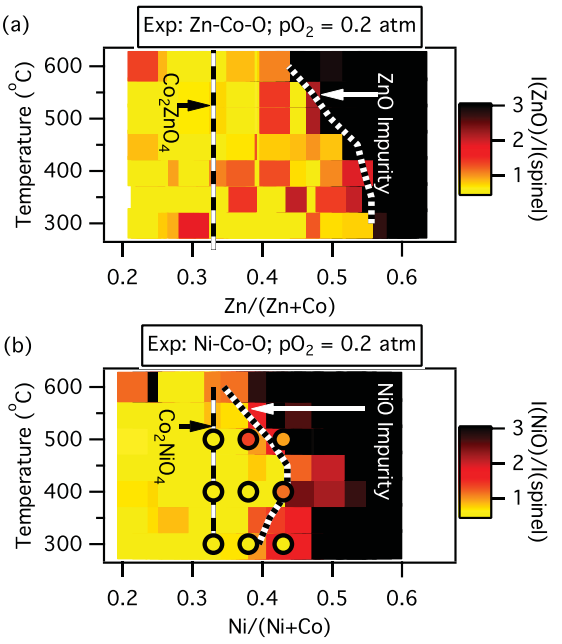

FIG. 3. (Color online) Experimental T-vs-composition crystalline phase purity maps for (a) Zn-Co-O and (b) Ni-Co-O. The color scales indicate the ratio of ZnO (002) and NiO (111) or NiO (200) peaks to the intensity of the spinel (311) or spinel (400) peaks, respectively. Closed circles in (b) are single-composition PLD results. The dashed lines indicate a nominal 2:1 spinel cation ratio, the dotted and dash-dotted lines indicate experimental onset of phase separation.

at ambient atmospheric pO_2. We note that these theoretic predictions for the pO_2-vs-T stability range do not take into account configurational entropy due to cation cross-substitution and nonequilibrium thin film growth effects. More details on the effects of deviation from thermodynamic equilibrium during the thin film growth on site occupancy in Co_2ZnO_4 were recently published elsewhere.[10]

The experimental nonequilibrium growth process increases pO_2-vs-T stability range of Co_2NiO_4 and increases solubility of Zn in Co_2ZnO_4 by 24 at.% compared to thermodynamic equilibrium. Thin film growth and annealing T and pO_2 conditions used to obtain single-phase Zn-Co-O and Ni-Co-O spinel samples are shown by symbols in Fig. 1. Experimental XRD maps for two typical Zn-Co-O and Ni-Co-O samples annealed at 350 °C are shown in Fig. 2, and the XRD results prior to the anneal were similar. Only spinel XRD peaks are present below 40 at.% in Ni-Co-O, indicating that nonequilibrium growth stabilizes the Co_2NiO_4 spinel phase [Fig. 2(b)]. Co_2ZnO_4 spinel phase [Fig. 2(a)] is stable up to 56 at.% Zn, which is almost twice its equilibrium solubility limit (<33 at.% Zn) that is calculated using Eq. (5). It was not possible to use our XRD results to show that Co_2ZnO_4 is a normal spinel and that Co_2NiO_4 is an inverse spinel due to similarity in the x-ray diffraction patterns caused by similar atomic numbers of Co, Ni, and Zn ions. However, recent results of anomalous x-ray diffraction (AXRD) experiments[27] as well as previous publications[11,12] confirm these statements. Nevertheless, in this paper, we refer to the crystallographic structure of both Zn-Co-O and Ni-Co-O samples using a common term spinel.

The T-vs-composition boundary between spinel phase and mixed phase have distinctly different shapes in the cases of air-annealed Zn-Co-O and Ni-Co-O, as shown in Fig. 3. The composition range in which Zn-Co-O single-phase spinel is stable monotonically decreases with increasing annealing temperature [dotted lines in Fig. 3(a)]. Despite being shifted by 24 at.% to higher Zn content, the shape of this boundary is in good qualitative agreement with previously published theoretic and bulk synthesis results.[4] In contrast to Zn-Co-O, the composition stability range of Ni-Co-O single phase spinel [Fig. 3(b)] has an unusual shape with a maximum at 400–450 °C. We hypothesize that annealing up to 400–450 °C in air increases composition stability range of Co_2NiO_4 spinel phase because, theoretically, Co_2NiO_4 is thermodynamically stable at much more oxidizing conditions [green/gray region in Fig. 1(b)] than those that were used for the thin film growth [yellow/light gray symbols in Fig. 1(b)]. The phase purity results obtained for the combinatorial Ni-Co-O samples [Fig. 3(b)] are consistent with the phase purity results obtained for the single-composition Ni-Co-O samples prepared by PLD [circles in Fig. 3(b)].

As a summary of this section, we found that sputtering and pulsed laser deposition stabilize Co_2NiO_4 thin films in spinel structure and stabilize Zn-rich off-stoichiometry in Co_2ZnO_4 (Figs. 1–3). These results do not contradict with theoretical predictions for the pO_2-vs-T-vs-composition stability range of the spinels, since such calculations assume thermodynamic equilibrium.

B. Electrical and optical properties

Conductivity, which is one of the two definitional metrics of transparent conductive oxides (TCOs), is strongly enhanced

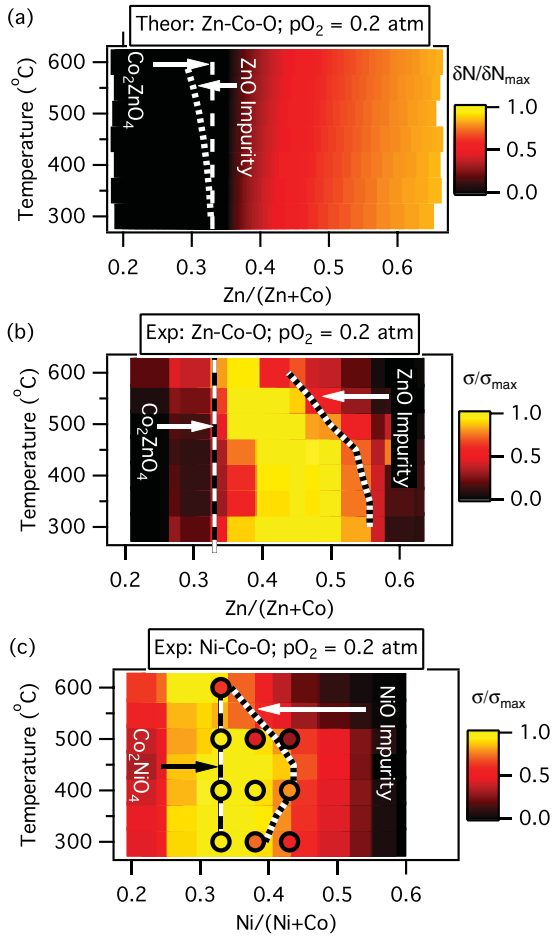

FIG. 4. (Color online) (a) Normalized theoretic nonequilibrium net acceptor density for Zn-Co-O. Dotted line in (a) indicates an onset of phase-separation in thermodynamic equilibrium. Normalized experimental conductivity maps for (b) Zn-Co-O and (c) Ni-Co-O, respectively. Closed circles in (c) are single-composition PLD results. The dotted lines in (b) and (c) indicate experimental onsets of phase separation. For (a)–(c) the dashed lines indicate a nominal 2:1 spinel cation ratio. All mapped quantities are normalized to maximum at different temperatures separately to emphasize their relation to the ideal 1:2 cation ratio (dashed lines) and to onset of phase separation (dotted lines).

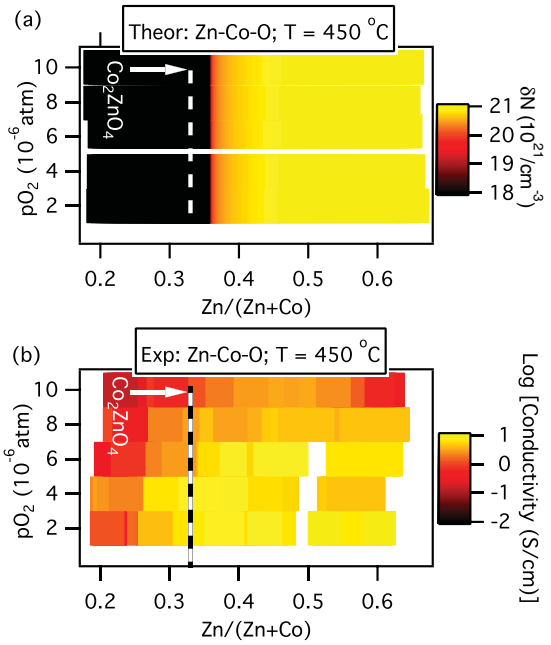

FIG. 5. (Color online) (a) Theoretical net acceptor density map for Zn-Co-O and (b) experimental conductivity maps for Zn-Co-O prepared at different pO_2. For both theory and experiment, the dashed lines indicate a nominal 2:1 spinel cation ratio.

when Zn atoms are incorporated in Zn-Co-O above equilibrium solubility limit [dotted line in Fig. 4(a)]. As shown in Fig. 4(a), the normalized net acceptor density [Eq. (9)] is predicted to sharply increase to 10^{20}–10^{21} cm^{-3} above Zn/(Zn + Co) = 0.33 composition [dashed line in Fig. 4(a)]. In this Zn-rich region, almost all Td sites (1/3 of all cation sites) are filled by Zn atoms, and the excess Zn atoms occupy Oh sites, thereby creating free holes. Normalized experimental conductivity in Zn-Co-O samples annealed in air also increases above Zn/(Zn + Co) = 0.33 composition [dashed line in Fig. 4(b)], but drops with further increase in Zn concentration due to ZnO phase separation [dashed line in Fig. 4(b)]. The maximum measured conductivity of Zn-Co-O is 5 S/cm for 44 at.% of Zn in the sample annealed at 400 °C, and there is a high-conductivity (>2 S/cm) region around this point with quite wide boundaries (35–55 at.% Zn below 500 °C). The conductivity mapping results for the unannealed Zn-Co-O samples deposited at varying substrate temperature are essentially the same as shown in Fig. 4(b) for the sample consequently annealed in air at various temperatures.

The maximum experimental conductivity of Ni-Co-O thin films is larger compared to that of Zn-Co-O thin films. For Ni-Co-O combinatorial and single-composition samples with Ni/(Ni + Co) = 0.33 annealed in air at 400–450 °C, the conductivities are 81 S/cm and 204 S/cm, respectively. These maximum values are surrounded by a broad (25–45 at.% below 500 °C) high-conductivity (>50 S/cm) region that is limited on the high-Ni side by phase separation of NiO [Fig. 4(c)], similar to the situation in Zn-Co-O [Fig. 4(b)]. Ni-Co-O samples deposited at varying substrate temperature in $pO_2 = 10^{-5}$ atm have the same chemical compositional spread of the high-conductivity region, but its high-temperature boundary is limited by 350 °C for the as-deposited samples, compared to 500 °C for the samples annealed in air. The maximum conductivity of Ni-Co-O (204 S/cm) reported in this paper is among the highest compared to other *p*-type TCOs, but its optimal chemical composition [Ni/(Ni + Co) = 0.33] is somewhat lower compared to the values reported before for this material [Ni/(Ni + Co) = 0.5].[28] One possible reason is higher nonequilibrium maximum concentration of Ni in the Ni-Co-O spinel structure, reported in Ref. 28.

Charge transport properties of Zn-Co-O are weakly sensitive to the oxygen partial pressure (Fig. 5), in contrast to oxygen sensitivity of other TCOs, such as *n*-type ZnO or *p*-type NiO. Zn-Co-O samples that were both grown in $pO_2 = 10^{-6}$–10^{-5} atm (Fig. 5) and annealed in $pO_2 = 0.2$ atm [Fig. 4(b)] had nearly the same (approximately a factor of 2 different) conductivity. These observations are consistent with the theoretic predictions that the oxygen

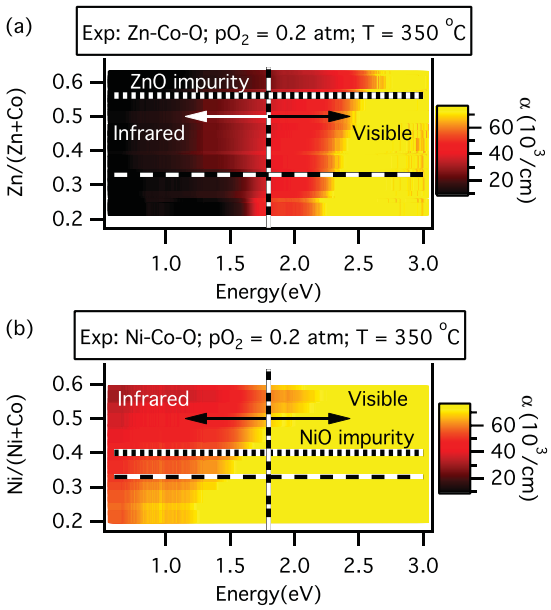

FIG. 6. (Color online) Experimental absorption coefficient maps for (a) Zn-Co-O and (b) Ni-Co-O annealed at 350 °C in air.

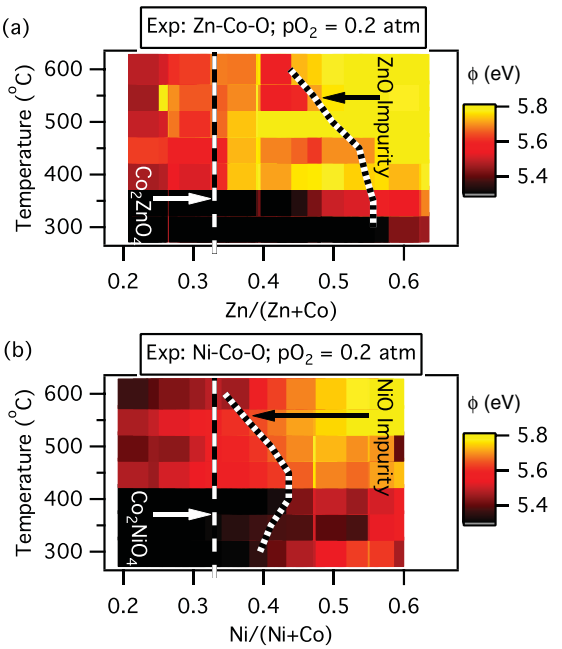

FIG. 7. (Color online) Experimental work function maps for (a) Zn-Co-O and (b) Ni-Co-O. The dashed lines indicate a nominal 2:1 spinel cation ratio, and the dotted lines indicate an onset of phase separation.

vacancies and interstitials have high formation energies in Co_2ZnO_4 [Eq. (8)] and hence are unlikely to form. We also note that, despite the nonequilibrium metastable character of Zn-Co-O and Ni-Co-O samples, their conductivity remains constant over the timescale of 1 year.

Transparency, which is the other definitional metric of transparent conductive oxides (TCOs), is in general smaller for Zn-Co-O and Ni-Co-O than for other TCOs. Experimental absorption coefficient maps in the visible and near-infrared range of the spectrum for Zn-Co-O and Ni-Co-O samples annealed at 350 °C are shown in Fig. 6. Addition of extra Zn and Ni shifts the optical absorption of Zn-Co-O and Ni-Co-O to higher energy, which improves the transparency of these materials, but even at the highest achievable Zn and Ni content, both spinels have rather strong absorption in visible and thus are on average <10% transparent to visible light at 500-nm film thickness. We found that the absorption maps shown in Fig. 6 for the samples annealed in air at 350 °C are the same for all other annealing temperatures and for as-deposited samples at various pO_2 and T. Despite quite high absorption values, transmittance of Zn-Co-O and Ni-Co-O materials can be increased by decreasing film thickness. For example, thin films of 7-nm thickness grown by pulsed laser deposition for use as hole-transport layers in organic photovoltaic devices have an average transmittance of 95%.[29]

As a summary of this section, we found that nonequilibrium substitution (i.e. off-stoichiometry) of divalent Zn on nominally trivalent Oh sites increases net hole density in Co_2ZnO_4 and Co_2NiO_4 thin films (Figs. 4 and 5), in good agreement with theoretic predictions. Off-stoichiometry also decreases the optical absorption of these materials (Fig. 6). These two findings demonstrate how cation off-stoichiometry can lead to p-type self doping and enhanced transparency of p-type TCOs, which is the main focus of this paper.

C. Work function and potential applications

Both Zn-Co-O and Ni-Co-O have relatively high work functions. Work function is an important property of TCOs used as contact layers in optoelectronics because it is determined both by the material's Fermi level (and thus, it is related to conductivity) and by its surface dipole (and thus, it partially determines the carrier extraction/injection properties of the TCO contact layer). For example, oxide materials with high work function are used as hole-transport layers in P3HT : PCBM bulk heterojunction organic photovoltaic devices.[30] Experimentally, the work function of Zn-Co-O samples annealed at 350–600 °C [Fig. 7(a)] increases from 5.6 to 5.9 eV with increasing amount of Zn. This trend can be partially attributed to downward shift in the position of the Fermi level, which also leads to increase in experimental conductivity [Fig. 4(b)]. For Ni-Co-O annealed at 400–600 °C [Fig. 7(b)], the range of variation of work functions is larger by 0.2–0.3 eV than in Zn-Co-O, but the absolute value of the work function is smaller by 0.1–0.2 eV than in Zn-Co-O. Above 600 °C and below 350–400 °C annealing temperature, as well as for as-deposited Zn-Co-O and Ni-Co-O samples aged for 6 months in air, the work function is somewhat smaller and much more scattered.

Zn-Co-O and Ni-Co-O materials have several potential advantages for practical technological applications in optoelectronics. The first advantage of these p-type Co-based spinels is the tolerance of their electrical properties to a broad range of chemical composition, oxygen pressure, and temperature during the processing (Figs. 4 and 5). The second advantage of these materials is the large value and the compositional tunability of their work function (Fig. 7). The third advantage is that Zn-Co-O and Ni-Co-O can be prepared in amorphous form

by RF sputtering at room temperature,[6,28] which makes these materials compatible with roll-to-roll processing on plastic substrates. An additional advantage of Zn-Co-O and Ni-Co-O is that they are isostructural in the spinels phase, so quaternary Zn-Ni-Co-O materials with tunable chemical composition and physical properties are possible.[31] The only apparent disadvantage of Zn-Co-O and Ni-Co-O materials is their limited transparency (Fig. 6). Nevertheless, these somewhat transparent materials can be used as hole transport layers in bulk heterojunction organic photovoltaic (OPV) devices, in which very thin (∼5–10 nm) layers are sufficient,[30,31] or as back-contact *p*-type membrane (window) layers[32] in inorganic thin film solar cells [CdTe, Cu(In,Ga)$(S,Se)_2$ (CIGS) and $Cu_2ZnSn(S,Se)_4$ (CZTS)], which also do not require full transparency.[33]

IV. SUMMARY

In summary, we found that high levels of *p*-type conductivity in Co_2ZnO_4 and Co_2NiO_4 oxides spinels can be achieved by off-stoichiometry induced by nonequilibrium thin film growth. Nonequilibrium growth also increased pO_2-T-composition stability range and improved optical transparency of Zn-Co-O and Ni-Co-O thin films. Furthermore, Co_2ZnO_4 and Co_2NiO_4 thin films have quite high work function. All these TCO metrics are relatively constant in the broad composition range; they are only weakly sensitive to oxygen partial pressure during the deposition or anneal and quite tolerant to the wide variation in the deposition or annealing temperature. We conclude that Co_2ZnO_4 and Co_2NiO_4 are technologically attractive for applications as thin functional *p*-type layers in optoelectronic devices.

ACKNOWLEDGMENTS

This work is supported by the US Department of Energy, Office of Science, Basic Energy Sciences, under Contract No. DE-AC36-08GO28308 to NREL as a part of the DOE Energy Frontier Research Center "Center for Inverse Design". The use of MPP capabilities at the National Energy Research Scientific Computing Center is gratefully acknowledged. The authors would like to thank P. A. Parilla for the assistance with high-throughput XRD and XRF data processing and N. E. Widjonarko and J. J. Berry for the assistance with the KP measurement setup.

*Corresponding author: 1617 Cole Blvd., Golden, CO 80401-3305; andriy.zakutayev@nrel.gov

†Current address: University of Colorado, Boulder, CO 80309, USA.

[1]Another widely used way of writing the spinel chemical formula is AB_2O_4. We write however, A_2BO_4, which is common for spinels with formal cation valencies $Z_A = 2$ and $Z_B = 4$ such as Mg_2TiO_4. The main reason for our choice is because the work presented here is part of a larger project that treats all A_2BX_4 compounds (not only spinels) in different structure types, including Olivine Fe_2SiO_4, β-K_2SO_4, or La_2CuO_4, for which A_2BX_4 is the generally used notation.

[2]V. Stevanovic, M. d'Avezac, and A. Zunger, J. Am. Chem. Soc. **133**, 11649 (2011).

[3]V. Stevanovic, M. d'Avezac, and A. Zunger, Phys. Rev. Lett. **105**, 075501 (2010).

[4]T. R. Paudel, S. Lany, M. d'Avezac, A. Zunger, N. H. Perry, A. R. Nagaraja, T. O. Mason, J. S. Bettinger, Y. Shi, and M. F. Toney, Phys. Rev. B **84**, 064109 (2011).

[5]T. R. Paudel, A. Zakutayev, V. Stevanović, S. Lany, M. d'Avezac, and A. Zunger, Adv. Funct. Mater. **21**, 4493 (2011).

[6]S. Kim, J. A. Cianfrone, P. Sadik, K.-W. Kim, M. Ivill, and D. P. Norton, J. Appl. Phys. **107**, 103538 (2010).

[7]H. Mizoguchi, M. Hirano, S. Fujitsu, T. Takeuchi, K. Ueda, and H. Hosono, Appl. Phys. Lett. **80**, 1207 (2002).

[8]M. Dekkers, G. Rijnders, and D. H. A. Blank, Appl. Phys. Lett. **90**, 021903 (2007).

[9]D. O. Scanlon and G. W. Watson, Phys. Chem. Chem. Phys. **13**, 9667 (2011).

[10]J. D. Perkins, T. R. Paudel, A. Zakutayev, P. F. Ndione, P.A. Parilla, D. L. Young, S. Lany, D. S. Ginley, A. Zunger, N. H. Perry, Y. Tang, M. Grayson, T. O. Mason, J. S. Bettinger, Y. Shi, and M. F. Toney, Phys. Rev. B **84**, 205207 (2011).

[11]O. Knop, K. I. G. Reid, R. Sutarno, and Y. Nakagawa, Can. J. Chem. **46**, 3463 (1968).

[12]K. Krezhovand and P. Konstantinov, J. Phys. Condens. Matter **5**, 9287 (1993).

[13]J. Osorio-Guillén, S. Lany, S. V. Barabash, and A. Zunger, Phys. Rev. Lett. **96**, 107203 (2006).

[14]K. Biswas and S. Lany, Phys. Rev. B **80**, 115206 (2009).

[15]S. Lany, J. Osorio-Guillén, and A. Zunger, Phys. Rev. B **75**, 241203(R) (2007).

[16]S. Lany and A. Zunger, Phys. Rev. B **78**, 235104 (2008).

[17]S. Lany and A. Zunger, Phys. Rev. Lett. **98**, 045501 (2007).

[18]P. E. Blöchl, Phys. Rev. B **50**, 17953 (1994).

[19]J. P. Perdew, K. Burke, and M. Ernzerhof, Phys. Rev. Lett. **77**, 3865 (1996).

[20]J. Paier, R. Hirschl, M. Marsman, and Ge. Kresse, J. Chem. Phys. **122**, 234102 (2005).

[21]S. L. Dudarev, S. Y. Savrasov, C. J. Humphreys, and A. P. Sutton, Phys. Rev. B **57**, 1505 (1998).

[22]H. Monkhorst and J. Pack, Phys. Rev. B **13**, 5188 (1976).

[23]S. Baroni and R. Resta, Phys. Rev. B **33**, 7017 (1986).

[24]J. D. Perkins, J. A. del Cueto, J. L. Alleman, C. Warmsingh, B. M. Keyes, L. M. Gedvilas, P. A. Parilla, B. To, D. W. Reade, and D. S. Ginley, Thin Solid Films **411**, 152 (2002).

[25]Y. Hishikawa, N. Nakamura, S. Tsuda, S. Nakano, Y. Kishi, and Y. Kuwano, Jpn. J. Appl. Phys. **30**, 1008 (1991).

[26]A. Zakutayev, F. J. Luciano IV, P. F. Ndione, P. A. Parilla, V. Bollinger, J. J. Berry, J. D. Perkins, and D. S. Ginley (unpublished).

[27]Y. Shi, P. F. Ndione, J. S. Bettinger, and M. F. Toney (unpublished).

[28]R. R. Owings, G. J. Exarhos, C. F. Windisch, P. H. Holloway, and J. G. Wen, Thin Solid Films **483**, 175 (2005).

[29]P. F. Ndione, J. J. Berry, and D. S. Ginley (unpublished).

[30]K. X. Steirer, J. P. Chesin, N. E. Widjonarko, J. J. Berry, A. Miedaner, D. S. Ginley, and D. C. Olson, Org. Electron. **11**, 1414 (2010).

[31]A. Zakutayev, J. D. Perkins, P. A. Parilla, N. E. Widjonarko, A. K. Sigdel, J. J. Berry, and D. S. Ginley, MRS Communications **1**, 23 (2011).

[32]J. A. Spies, R. Schafer, J. F. Wager, P. Hersh, H. A. S. Platt, D. A. Keszler, G. Schneider, R. Kykyneshi, J. Tate, X. Liu, A. D. Compaan, and W. N. Shafarman, Sol. Energy Mater. Sol. Cells **93**, 1296 (2009).

[33]W. Jaegermann, A. Klein, and T. Mayer, Adv. Mater. **21**, 4196 (2009).